Published Online: 19 May, 2008 | Supp Info: http://doi.org/10.1083/jcb.200711058

Myofiber integrity depends on desmin network targeting to Z-disks and costameres via distinct plectin isoforms

Patryk Konieczny,[1] Peter Fuchs,[1] Siegfried Reipert,[1] Wolfram S. Kunz,[2,3] Anikó Zeöld,[1] Irmgard Fischer,[1] Denise Paulin,[4] Rolf Schröder,[5] and Gerhard Wiche[1]

[1]Max F. Perutz Laboratories, Department of Molecular Cell Biology, University of Vienna, A-1030 Vienna, Austria
[2]Department of Epileptology and [3]Life & Brain Center, University of Bonn, D-53105 Bonn, Germany
[4]Biologie Moléculaire de la Différenciation, Université Paris 7, 75005 Paris, France
[5]Institute of Neuropathology, Friedrich-Alexander University, D-91054 Erlangen, Germany

Dysfunction of plectin, a 500-kD cytolinker protein, leads to skin blistering and muscular dystrophy. Using conditional gene targeting in mice, we show that plectin deficiency results in progressive degenerative alterations in striated muscle, including aggregation and partial loss of intermediate filament (IF) networks, detachment of the contractile apparatus from the sarcolemma, profound changes in myofiber costameric cytoarchitecture, and decreased mitochondrial number and function. Analysis of newly generated plectin isoform–specific knockout mouse models revealed that IF aggregates accumulate in distinct cytoplasmic compartments, depending on which isoform is missing. Our data show that two major plectin isoforms expressed in muscle, plectin 1d and 1f, integrate fibers by specifically targeting and linking desmin IFs to Z-disks and costameres, whereas plectin 1b establishes a linkage to mitochondria. Furthermore, disruption of Z-disk and costamere linkages leads to the pathological condition of epidermolysis bullosa with muscular dystrophy. Our findings establish plectin as the major organizer of desmin IFs in myofibers and provide new insights into plectin- and desmin-related muscular dystrophies.

Introduction

Intermediate filament (IF)-based cytoskeletal linker proteins (cytolinkers) comprise a growing number of proteins that play a major role in maintaining cell integrity, especially in tissues that are exposed to constant mechanical stress such as skin and skeletal muscle. Because of its versatility, abundance, and widespread distribution, plectin, a 500-kD protein with multiple binding activities, plays a key role among cytolinkers (Wiche, 1998). It cross-links cytoskeletal filament systems and connects them to plasma membrane junctional complexes and organelles in a wide variety of cell types. Moreover, plectin creates scaffolding platforms for signaling molecules, exceeding its cytolinker function (Osmanagic-Myers et al., 2006).

Correspondence to G. Wiche: gerhard.wiche@univie.ac.at

Abbreviations used in this paper: β-DG, β-dystroglycan; CNF, centrally nucleated fiber; COX, cytochrome c oxidase; CSA, cross-sectional area; DGC, dystrophin–glycoprotein complex; DRM, desmin-related myopathy; EBD, Evans blue dye; EB-MD, epidermolysis bullosa with muscular dystrophy; EDL, extensor digitorum longus; H & E, hematoxylin and eosin; IF, intermediate filament; MCK, muscle creatine kinase; nNOS, neuronal nitric oxide synthase; SDH, succinate dehydrogenase; WT, wild type.

The online version of this paper contains supplemental material.

A unique feature of plectin is its transcript diversity, which is largely based on different N-terminal sequences encoded by alternatively spliced first exons (Fuchs et al., 1999). Of the dozen isoforms identified to date, the ones most prominently expressed in skeletal and cardiac muscle are plectin 1, 1b, 1d, and 1f (Fuchs et al., 1999). Recently, we found that plectin isoforms 1 and 1f are localized at costameres (Rezniczek et al., 2007), which are protein assemblies surrounding the contractile apparatus and linking it via the sarcolemma to the extracellular lattice (Bloch et al., 2002; Ervasti, 2003). In contrast, plectin 1d specifically associated with Z-disks of cultured myotubes, whereas plectin 1b colocalized with mitochondria (Rezniczek et al., 2003, 2007).

Mutations in the plectin gene cause epidermolysis bullosa with muscular dystrophy (EB-MD), EB simplex Ogna, and EB with pyloric atresia (Pfendner et al., 2005). EB-MD is characterized by skin blistering and late-onset, progressive muscular dystrophy. Moreover, plectin deficiency in mice leads to early death in postnatal development as a consequence of internal blistering of the oral cavity that disallows food uptake (Andrä et al., 1997;

The Rockefeller University Press $30.00
J. Cell Biol. Vol. 181 No. 4 667–681
www.jcb.org/cgi/doi/10.1083/jcb.200711058

Ackerl et al., 2007). In addition to skin blistering, mutant mice show abnormalities in skeletal and cardiac muscle (Andrä et al., 1997); however, the cause of these pathological changes remains elusive.

Desmin filaments form the most prominent IF network in striated muscle. They surround myofibrils at the level of Z-disks and extend to the sarcolemma, intercalated disks, and various organelles, including nuclei and mitochondria (Capetanaki et al., 2007). Mice lacking desmin develop muscular dystrophy characterized by a loss of muscle integrity (Li et al., 1996; Milner et al., 1996), disorganized mitochondrial networks (Milner et al., 2000), and compromised endurance performance (Haubold et al., 2003). Because plectin has been shown to bind to desmin (Reipert et al., 1999) and has been implicated in linking desmin IFs to Z-disks and the sarcolemma (Hijikata et al., 1999; Rezniczek et al., 2007), we hypothesized that pathological alterations observed in striated muscle of plectin-null mice could be caused by the disruption of desmin IF network organization. Plectin-null mice were unsuitable for assessing this hypothesis because of their early death. Therefore, we took a conditional knockout approach and ablated plectin expression only in striated muscle. In addition, to distinguish between isoform-specific functions, we used two newly generated mouse lines as well as one previously generated mouse line that were deficient in either plectin isoform 1d, 1b, or 1. The full repertoire of mouse models comparatively investigated in this study also comprised a desmin-null and a newly generated desmin/plectin isoform 1d double knockout line.

We show that plectin deficiency causes detachment of desmin IFs from Z-disks, costameres, mitochondria, and nuclei, leading to the formation of desmin aggregates of distinct morphology and in distinct cytoplasmic compartments, depending on which plectin isoforms are missing. Furthermore, we show that synemin and syncoilin, proteins that have been proposed to anchor desmin IFs to Z-disks and costameres (Bellin et al., 2001; Newey et al., 2001), in the absence of plectin, are insufficient for desmin IF docking. As a consequence, the sarcolemma becomes detached from the contractile apparatus, Z-disks show misalignments, fibers enlarge, and aggregation and loss of mitochondria occur, with mitochondria-rich soleus being the most severely affected type of muscle. Additionally, profound changes in the costameric lattice of plectin-deficient muscle fibers were detected, including altered levels and locations of proteins with key roles in muscle signaling, such as β-dystroglycan (β-DG), caveolin 3, and neuronal nitric oxide synthase (nNOS). Our data suggest that the pathological conditions of EB-MD patients have their etiology in structural changes as well as signaling alterations.

Results

Plectin deficiency in striated muscles leads to reduced endurance performance and increased mortality

To ablate plectin expression specifically in striated muscle, homozygous and heterozygous plectin floxed mice ($ple^{f/f}$, $ple^{f/+}$, and $ple^{f/-}$; collectively referred to as f-ple) were bred to muscle creatine kinase (MCK)-Cre mice expressing the Cre transgene under the control of the MCK promoter (Bruning et al., 1998). Conditional knockout mice that were obtained ($ple^{\Delta/\Delta}$ and $ple^{\Delta/-}$; referred to as cKO-ple) were born at Mendelian ratios and did not show any overt phenotype within the first months of life. Plectin expression was efficiently ablated in mature skeletal muscle fibers and cardiomyocytes (Fig. S1, A–C, available at http://www.jcb.org/cgi/content/full/jcb.200711058/DC1); however, plectin-positive signals were observed in connective tissue cells (Fig. S1 C, arrowheads) and regenerating fibers (Fig. S1 C, arrows), presumably because of the late onset of MCK expression (Washabaugh et al., 1999). Starting from 6 mo of life, cKO-ple mice exhibited decreasing survival rates (Fig. S2 A), and when subjected to voluntary wheel-running, showed a progressive decrease in endurance performance (Fig. S2, C and D). Furthermore, at 16 mo of age, some cKO-ple mice displayed muscle mass loss and kyphosis (Fig. S2 B). Neither in sedentary nor in voluntarily wheel-running mice were dilated or hypertrophic cardiomyopathies observed (unpublished data). Similarly, no obvious phenotype was observed in the morphology of extensor digitorum longus (EDL), which is mostly glycolytic (unpublished data). In contrast, 6-mo-old cKO-ple mice exhibited pathological alterations of mitochondria-rich soleus, manifesting as a pale appearance clearly visible from the eighth week of age and increased weight (Fig. 1 A).

Onset and progressivity of pathological changes are dependent on the type of muscle

To identify structural alterations of skeletal muscle fibers and cardiomyocytes in cKO-ple mice, muscle sections were stained with hematoxylin and eosin (H & E). In the soleus of 8-wk-old animals, numerous necrotic and centrally nucleated fibers (CNFs), representing regenerating and immature fibers, were observed (Fig. 1 B). In addition, the inner structure of fibers appeared disorganized, and vast eosinophylic inclusions were observed underneath the sarcolemma (Fig. 1 B, inset). In older mice, this phenotype was accompanied by hypertrophic and split fibers and a marked increase of connective tissue (Fig. 1 B, Sirius red staining). Furthermore, focal subsarcolemmal damage and the detachment of the sarcolemma from the contractile apparatus were visualized by electron microscopy of soleus and diaphragm (Fig. 1 C). The quantification of toluidine blue–stained, epoxy resin–embedded soleus sections from 8-wk-old cKO-ple mice revealed that ∼61% of the fibers showed focal detachments (Fig. 1 C). Indicative of a more severe phenotype under stress conditions, in 3-mo-old exercised (voluntarily wheel-running) cKO-ple mice, the amount of CNFs in soleus was markedly higher (∼35%) than in sedentary (∼22%) cKO-ple littermates (Fig. 1 D). In 12-mo-old exercised cKO-ple mice, the number of soleus CNFs reached ∼45% (Fig. 1 E). Necrotic, regenerating, split, and hypertrophic fibers could also be observed in EDL and diaphragm (unpublished data). The phenotype, however, was much less severe in these cases (Fig. 1 E). No signs of pathology were observed in the hearts of 12-mo-old cKO-ple mice. In contrast, the hearts of 16-mo-old mice showed markedly increased

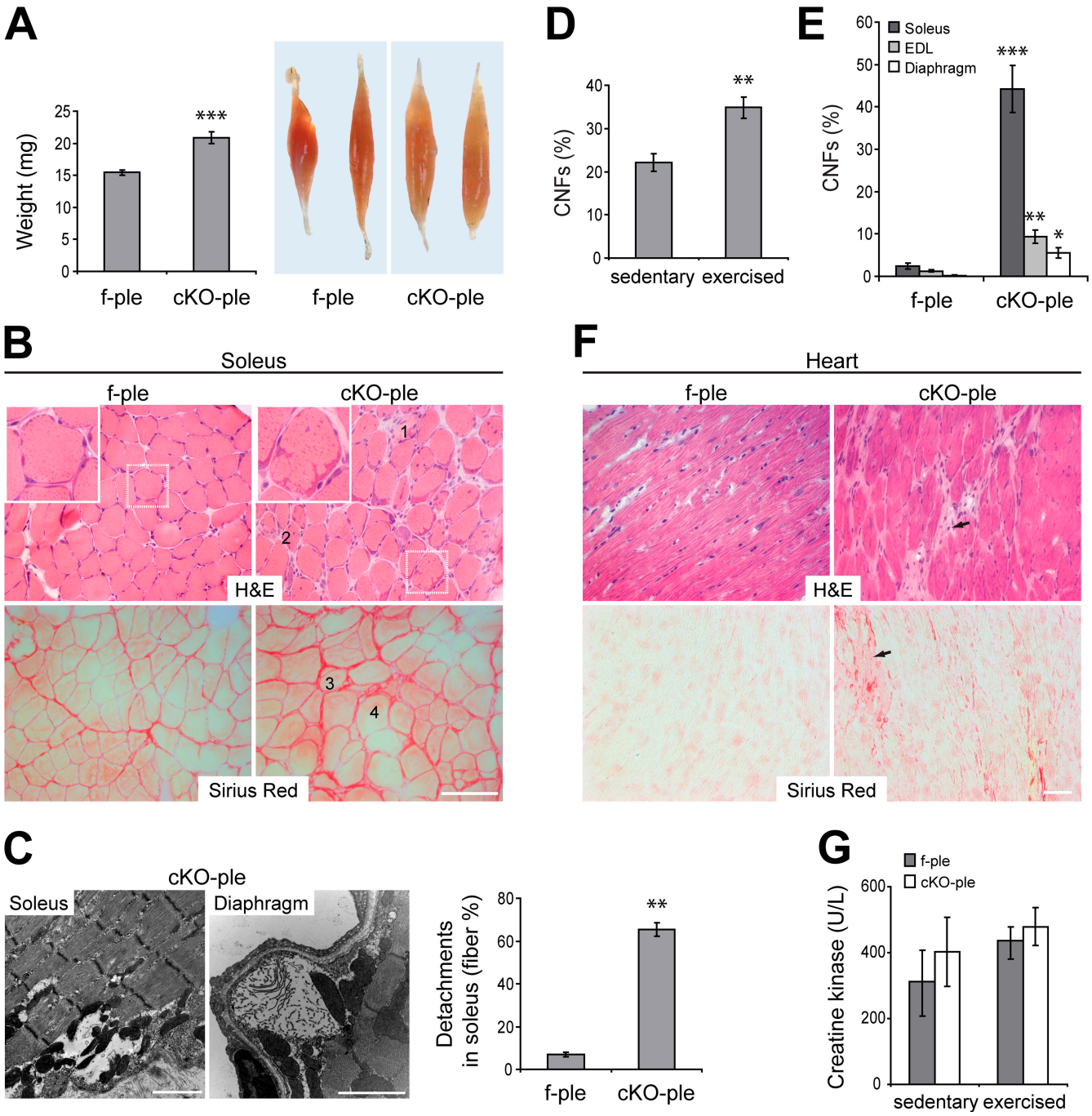

Figure 1. **Onset and progressivity of pathological alterations in cKO-ple mice is muscle type dependent.** (A) Statistical weight analyses of soleus dissected from 6-mo-old f-ple and cKO-ple mice (n = 14). Also note the pale appearance of cKO-ple compared with f-ple specimens. (B) Frozen sections of f-ple and cKO-ple soleus from 8-wk-old (H & E) and 6-mo-old mice (Sirius red). In cKO-ple samples, note the subsarcolemmal dense structures (inset), and numerous necrotic (1), centrally nucleated (2), split (3), and hypertrophic (4) fibers. Sirius red staining additionally revealed extensive fibrosis in cKO-ple samples. Boxed areas indicate representative fibers shown in detail as insets. (C) Electron micrographs showing detachment of the sarcolemma from the interior of cKO-ple fibers (soleus and diaphragm) and quantification of affected fibers using toluidine blue–stained sections of soleus. (D) Percentages of CNFs in 3-mo-old sedentary and exercised cKO-ple littermates (n = 15). (E) Diagram representing percentages of CNFs in soleus (n = 16), EDL (n = 17), and diaphragm (n = 11) of f-ple and cKO-ple mice. (F) Heart sections of 16-mo-old cKO-ple mice stained with H & E or Sirius red. Note the increased connective tissue formation (arrows), which is indicative of cardiomyocyte degeneration. (G) Serum creatine kinase levels of sedentary (8-wk-old; n = 10) or exercised (6-mo-old; n = 4) f-ple and cKO-ple mice. Bar graphs show mean values ± SEM. *, $P < 0.05$; **, $P < 0.01$; ***, $P < 0.001$. Bars: (B and F) 100 µm; (C) 2 µm.

amounts of connective tissue, which indicates the degeneration of cardiomyocytes (Fig. 1 F, arrows).

We next investigated whether the barrier function of cKO-ple myofibers is preserved by measuring the creatine kinase level in serum and by assessing penetration of Evans blue dye (EBD) into muscle fibers (Straub et al., 1997). However, creatine kinase levels showed no significant differences between either sedentary or exercised f-ple and cKO-ple mice (Fig. 1 G),

nor was an accumulation of EBD found in the interior of cKO-ple soleus or EDL fibers (unpublished data). This indicated that the sarcolemmal integrity of cKO-ple myofibers was unaffected.

Lack of plectin causes aggregation and loss of IFs, Z-disk misalignments, and profound changes in the costameric lattice

In skeletal muscle of f-ple mice, desmin IFs typically were located at the level of Z-disks and underneath the sarcolemma (Fig. 2 A, a and c), overlapping to a high extent with plectin (Fig. 2 A, a). In plectin-deficient fibers, this typical pattern was lost and desmin aggregates became apparent in the sarcoplasm (Fig. 2 A, d, arrow) and in the subsarcolemmal region (Fig. 2 A, d, arrowhead). Furthermore, desmin appeared to be reduced in the interior of fibers, whereas it was increased at the sarcolemma. In plectin-deficient cardiomyocytes as well, the cross-striated desmin pattern was lost (Fig. 2 B, b) and focal disorganization of the contractile apparatus was observed (Fig. 2 B, f, inset). In contrast, the intercalated disk structures of cardiomyocytes appeared to be intact, with both desmin and desmoplakin showing normal patterns (Fig. 2 B, b and d, respectively). Thus, the mild cardiac phenotype of cKO-ple mice, as compared with that of $des^{-/-}$ mice (Li et al., 1996; Milner et al., 1996; Thornell et al., 1997), most likely reflects a functional intercalated disk anchorage of desmin IFs through desmoplakin. This notion is consistent with the observation that overexpression of a desmoplakin mutant protein with an incapacitated IF-binding site leads to the detachment of desmin IFs from desmosomes, ultrastructural changes of intercalated disks, and severe cardiomyopathy (Yang et al., 2006).

A role in linking desmin IFs to the sarcolemma and Z-disks has previously been attributed to syncoilin (Newey et al., 2001) and synemin (Bellin et al., 2001). In skeletal muscles of f-ple mice, both proteins colocalized with desmin IFs at Z-disks and underneath the sarcolemma (Fig. 2 C, a and c). Intriguingly, in the absence of plectin, synemin and syncoilin lost their typical distribution and coaggregated with desmin IFs, predominantly in the subsarcolemmal region (Fig. 2 C, b and d).

To optimally visualize protein structures in subsarcolemmal (costameres) and perinuclear regions, we performed an immunohistochemical analysis of teased EDL fibers (Figs. 2 D and 3 A). In such specimens, colocalization of plectin and desmin was revealed in both costameres and longitudinal perinuclear structures; the latter occasionally formed a continuous band with a row of nuclei (Fig. 2 D). Remarkably, in the absence of plectin, desmin lost its costameric and perinuclear distribution and was found to form vast, longitudinal aggregates (Fig. 2 D, b). Additionally, in all fibers of 4-mo-old cKO-ple mice, α-actinin staining clearly showed misalignment of sarcomeric units (Fig. 2 D, d). In f-ple teased fibers, the desmin signal overlapped with those of syncoilin and synemin at costameric structures overlying Z-disks (Fig. 3 A, arrowheads) and/or perpendicular longitudinal lines (Fig. 3 A, arrows). Moreover, it colocalized with cytokeratin IFs and the components of the dystrophin–glycoprotein complex (DGC), such as β-DG, dystrophin, nNOS, and syntrophin. In contrast, the distribution of caveolin 3 was mostly complementary to that of desmin. In cKO-ple fibers, the localization of all these proteins was profoundly altered, with synemin and syncoilin coaggregating with desmin, and the other proteins spreading throughout the subsarcolemmal region (Fig. 3 A). A partially retained cytokeratin network pattern (Z-disk overlying as well as longitudinal structures) observed in fibers revealing desmin aggregates suggested that plectin was dispensable for cytokeratin network anchorage at the sarcolemma (Ursitti et al., 2004). Regarding the proposed role of syncoilin and synemin in linking desmin IFs to the sarcolemma and to Z-disks, these results implied that in the absence of plectin, the linkages formed by these proteins were too weak to sustain the desmin-anchoring function.

Next, we prepared gastrocnemius total lysates and membrane fractions (microsomes) from hind leg muscles of f-ple and cKO-ple mice and probed them for IF and costameric protein levels. Although the levels of total desmin (and synemin) IFs were clearly decreased in lysates (Fig. 3 B), in the microsomal fraction, desmin was markedly increased (Fig. 3 C). This confirmed the immunofluorescence microscopy data showing accumulations of IFs underneath the sarcolemma (Fig. 2, A and C). Furthermore, the relative amounts of spectrin, integrin β1 and its associated proteins talin and vinculin, and DGC proteins (β-DG, caveolin 3, dystrophin, nNOS, syntrophin, and utrophin) were increased in gastrocnemius lysates and/or microsomal fractions of cKO-ple mice. The highest difference in protein levels between cKO-ple and f-ple muscles was observed for caveolin 3, which in mutant samples reached >200% of control levels. Among the proteins tested, α-actinin was an exception, as it was decreased in the membrane fraction of cKO-ple mice to a level of ∼61% compared with f-ple mice, whereas it was unchanged in total lysates, which suggests inefficient anchoring of the α-actinin–based cytoskeleton to the sarcolemma. This result was in agreement with the observed focal detachments of the sarcolemma from the contractile apparatus (Fig. 1 C).

Plectin deficiency leads to disruption of the mitochondrial network combined with dysfunction and loss of mitochondria

As the organization of the mitochondrial network is altered in desmin-deficient ($des^{-/-}$) mice (Milner et al., 2000), we examined the integrity and localization of mitochondria in cKO-ple muscles. In control f-ple soleus and EDL, succinate dehydrogenase (SDH) staining (Fig. 4 A, a and b) and immunofluorescence microscopy (Fig. 4 B, a and b; and Fig. 4 C, a) revealed evenly distributed mitochondria throughout the sarcoplasm, with a slight accumulation in subsarcolemmal regions in mitochondria-rich fibers (Fig. 4 A, a and b, arrows). Mitochondria only partially colocalized with desmin networks (Fig. 4 B, a and b), and analysis of longitudinal sections revealed overlapping of plectin, desmin, and mitochondria at the level of Z-disks (Fig. 4 C, a, arrow; and not depicted). In both, cKO-ple and $des^{-/-}$ mice (Fig. 4 A and B, c–f; and Fig. 4 C, b and c), the mitochondrial signal appeared significantly reduced (compare Fig. 4 A, a and b, with Fig. 4 A, c–f). Also, mitochondria were no longer associated with Z-disks (Fig. 4 C, b and c), and conspicuous focal aggregates in sarcoplasmic and subsarcolemmal regions were

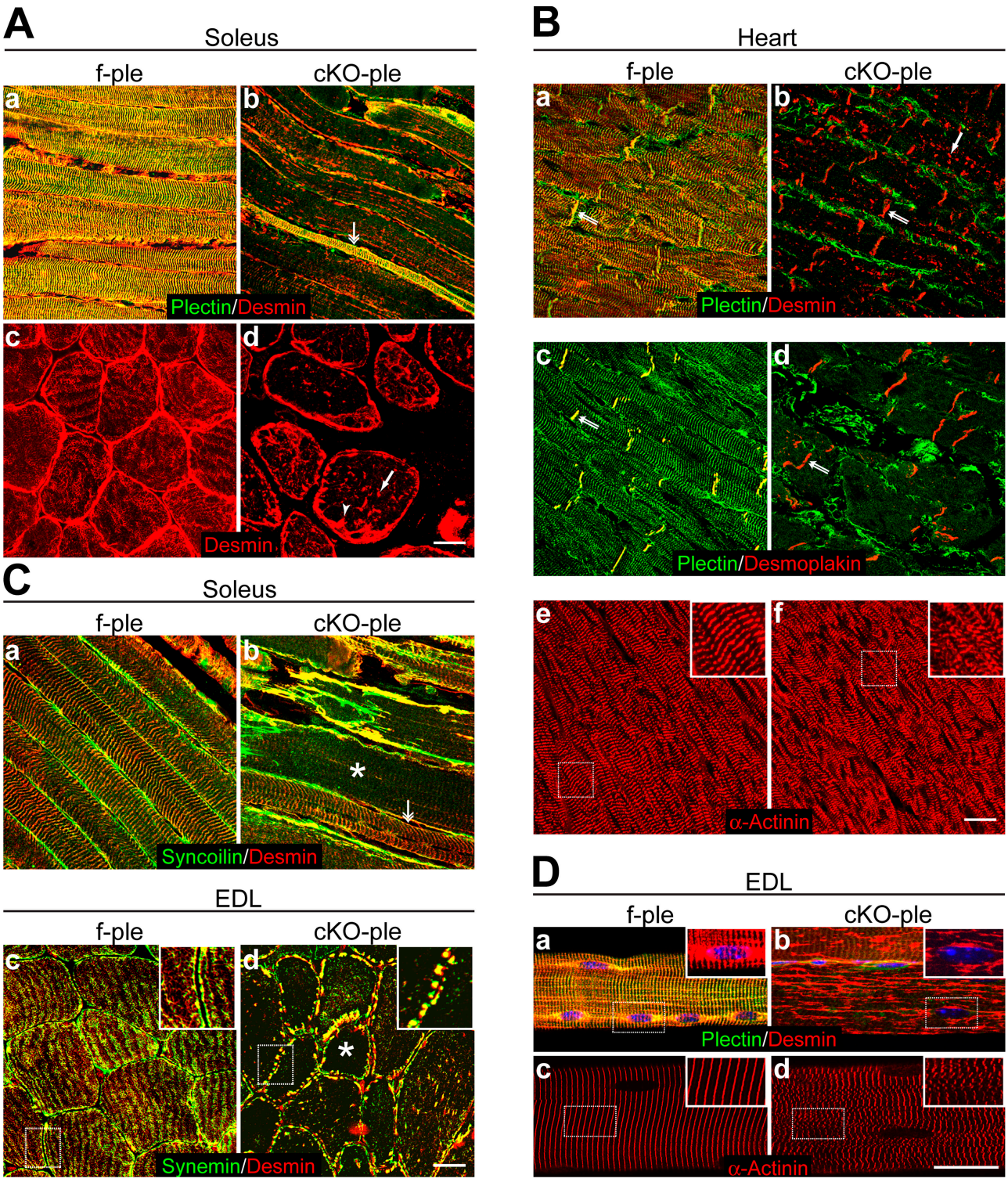

Figure 2. **Lack of plectin causes aggregation of IFs and disorganization of the contractile apparatus.** (A) Soleus f-ple (a and c) and cKO-ple (b and d) sections double immunolabeled for plectin and desmin (a and b) or stained for desmin alone (c and d). Note, desmin aggregates in the fiber interior (d, arrow) and accumulates along the sarcolemma (d, arrowhead) in plectin-negative fibers. The double-headed arrow in panel b represents a plectin-positive fiber with a preserved desmin-positive pattern. (B) f-ple (a, c, and e) and cKO-ple (b, d, and f) heart sections immunolabeled using antibodies to proteins as indicated. In cKO-ple cardiomyocytes, note the aggregates of desmin (b, arrow) and misaligned Z-disks (f, inset) as well as the seemingly preserved intercalated disk structures (double arrows). (C) f-ple (a and c) and cKO-ple (b and d) soleus longitudinal (a and b) and EDL cross sections (c and d) stained for proteins as indicated. Asterisks indicate fibers devoid of IFs in the fiber interior. The double-headed arrow in panel b represents a CNF with preserved IF pattern. The dotted boxes in panels c and d indicate areas shown magnified in the insets. (D) Immunofluorescence microscopy of teased fibers from f-ple (a and c) and cKO-ple (b and d) EDL revealing massive longitudinal desmin aggregates (b) and misaligned α-actinin–positive costameres (d, inset) in cKO-ple mice. No misalignments were observed in the case of f-ple costameres (c, inset). Note also the close association of desmin IFs with f-ple nuclei (a, inset) but their detachment from cKO-ple nuclei (b, inset). Dotted boxes indicate areas shown magnified in insets. Bars, 20 μm.

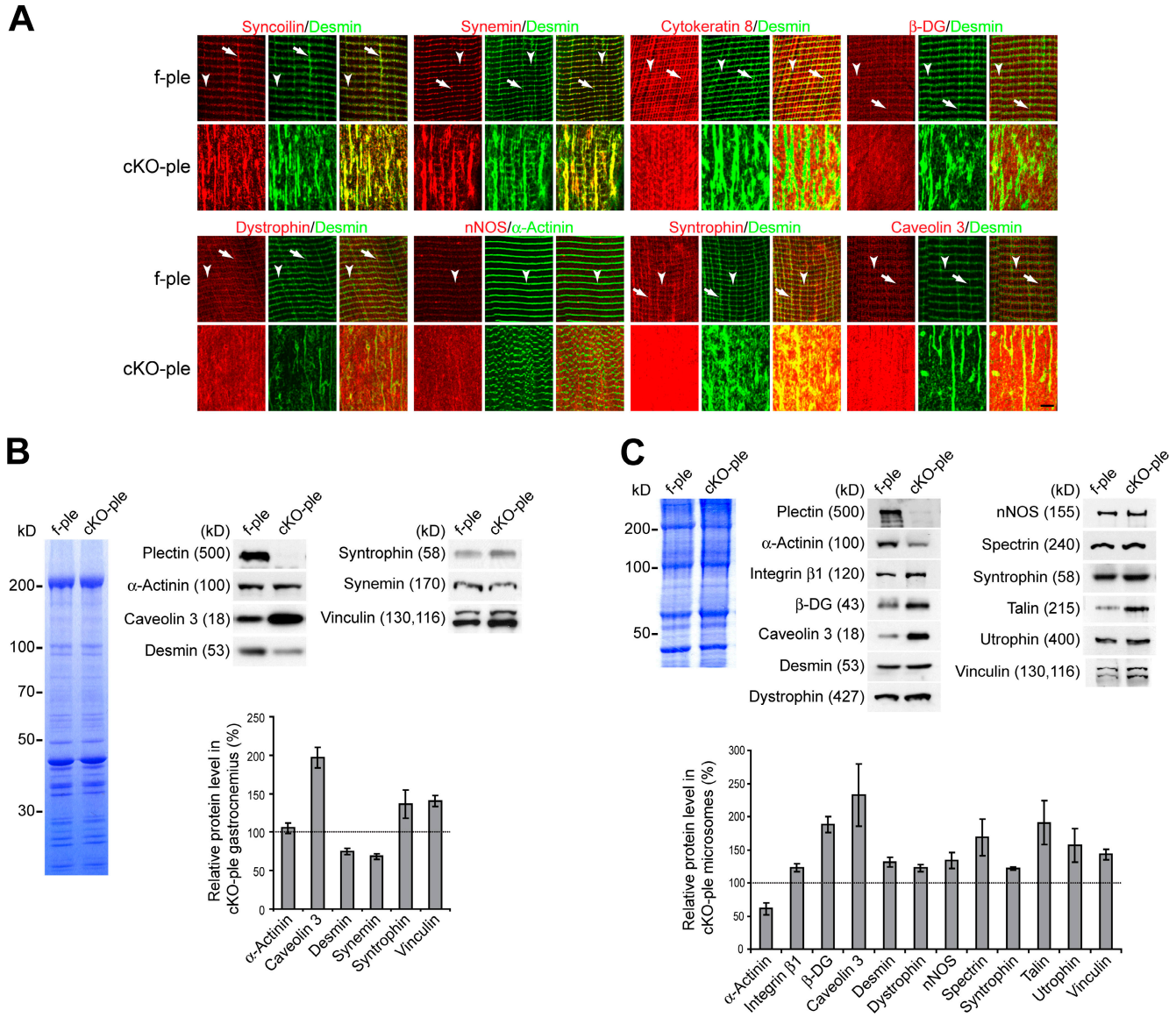

Figure 3. **Loss of IFs and profound changes in the costameric lattice of plectin-deficient muscles.** (A) Representative regions of teased EDL fibers from 4-mo-old f-ple and cKO-ple mice stained for proteins as indicated. Arrowheads and arrows indicate Z-disk–aligned and perpendicular longitudinal desmin-positive costameric structures, respectively. In f-ple fibers, note the colocalization of desmin IFs with syncoilin, synemin, cytokeratin 8, β-DG, dystrophin, nNOS, and syntrophin but not with caveolin 3. In cKO-ple fibers, all costameric marker proteins show profoundly changed localization patterns. Bar, 5 µm. (B and C) Quantitative immunoblotting analysis of gastrocnemius lysates from three 6-mo-old mice per genotype (B) and of microsomal fractions from at least three gel runs (C). Loading was normalized to total protein contents (Coomassie-stained gels). Bar graphs represent mean values ± SEM.

observed. Accumulations of mitochondria underneath the sarcolemma were especially pronounced in $des^{-/-}$ soleus fibers (Fig. 4 A, e, inset), in accordance with previously published data (Milner et al., 2000). Interestingly, in plectin-deficient fibers from both soleus and EDL, sarcoplasmic mitochondrial aggregates only partially overlapped with those of desmin (Fig. 4 B, c and d). The formation of massive mitochondrial aggregates underneath the sarcolemma of cKO-ple muscle fibers was also shown by electron microscopy (Fig. 4 D, a and b). Additionally observed pathological changes included misaligned Z-disks combined with loss of mitochondria from Z-disks (Fig. 4 D, a and c) and internal lysis of the organelles (not depicted). As shown by staining serial sections of soleus for SDH, cytochrome *c* oxidase (COX), H & E, and myosin ATPase, subsarcolemmal mitochondrial accumulations were independent of the fiber type (Fig. S3 B, available at http://www.jcb.org/cgi/content/full/jcb.200711058/DC1). Moreover, an increased mitochondrial subsarcolemmal signal corresponded with eosin-positive accumulations (Figs. 1 B and S3 B).

To quantitatively estimate the amount of mitochondria in cKO-ple muscles, the expression levels of mitochondrial marker proteins (porin, ATP synthase, and cytochrome *c*) were measured in gastrocnemius and EDL (Fig. 4 E). Levels of these proteins were found diminished to ~74% (ATP synthase), ~71% (porin), and ~67% (cytochrome *c*). Importantly, when the activities of citrate synthase and respiratory complexes I and IV were biochemically measured in soleus, decreases to ~63%, ~69%, and ~93%, respectively, were observed (Fig. 4 F).

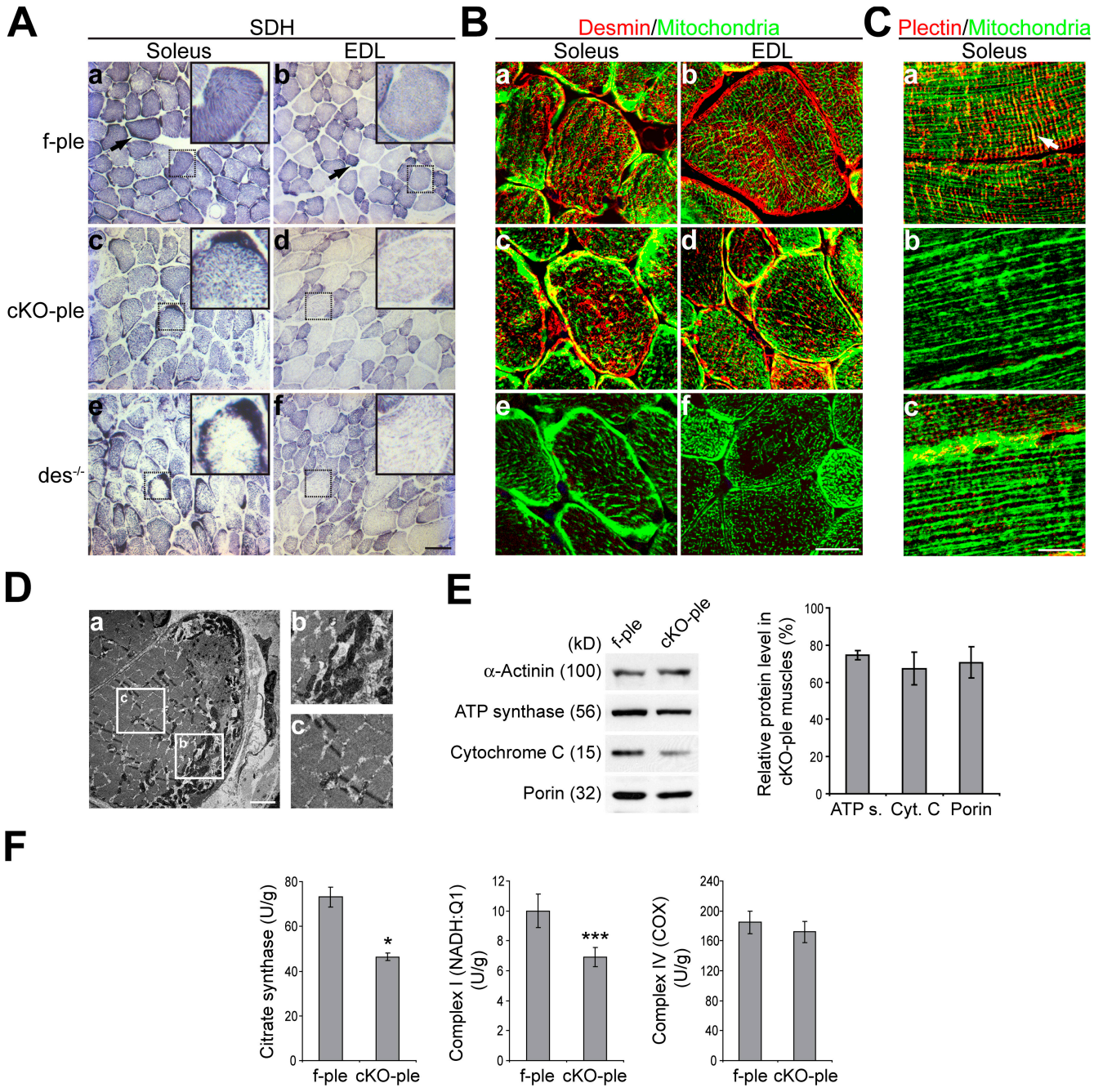

Figure 4. **Plectin deficiency leads to mitochondrial network disruption accompanied by reduction and dysfunction of mitochondria.** (A) Soleus and EDL cross sections stained for SDH. Insets show close-ups of representative fibers (boxed). Arrows in panels a and b indicate mitochondria-rich fibers. (B and C) Immunofluorescence microscopy of soleus and EDL cross sections immunostained for desmin and mitochondria (B) and soleus longitudinal sections labeled for plectin and mitochondria (C). Note the colocalization of plectin and mitochondria along Z-disks in f-ple fibers (C, a, arrow) and the thick, longitudinal mitochondrial aggregates in cKO-ple and des$^{-/-}$ fibers (C, b and c). (D) Electron microscopy showing cytoplasmic aggregates of mitochondria (a and b), scarce association of mitochondria with Z-disks, and Z-disk misalignments (a and c); panels b and c are magnifications of the boxed areas in panel a. (E) Quantitative immunoblotting of f-ple and cKO-ple gastrocnemius and EDL lysates. Data shown in left panel are from gastrocnemius; the bar graph (right) represents pooled data from gastrocnemius and EDL relative to f-ple muscle (100%). α-actinin was used as a loading control. Data were collected from at least five mice per genotype. Values represent means ± SEM. (F) Biochemical analysis of mitochondrial respiratory activities. Citrate synthase, complex I (NADH–Q1), and complex IV (COX) were measured in f-ple and cKO-ple soleus from 8-wk-old mice (n = 12). Mean values (U/g wet weight) ± SEM are shown. *, P < 0.05; ***, P < 0.001. Bars: (A) 50 µm; (B and C) 20 µm; (D) 2 µm.

Thus, morphological and biochemical analyses both indicated a reduced number of mitochondria in cKO-ple muscles. In addition, the fact that the relative activity of complex I showed a decrease to a much lower level than that of complex IV suggested dysfunctional cKO-ple mitochondria.

Loss of plectin isoform 1d, but not 1b or 1, results in pathological alterations

Because of their localization at mitochondria and Z-disks, respectively (Rezniczek et al., 2003, 2007), plectin isoforms 1b and 1d were strong candidates for playing a role in desmin filament

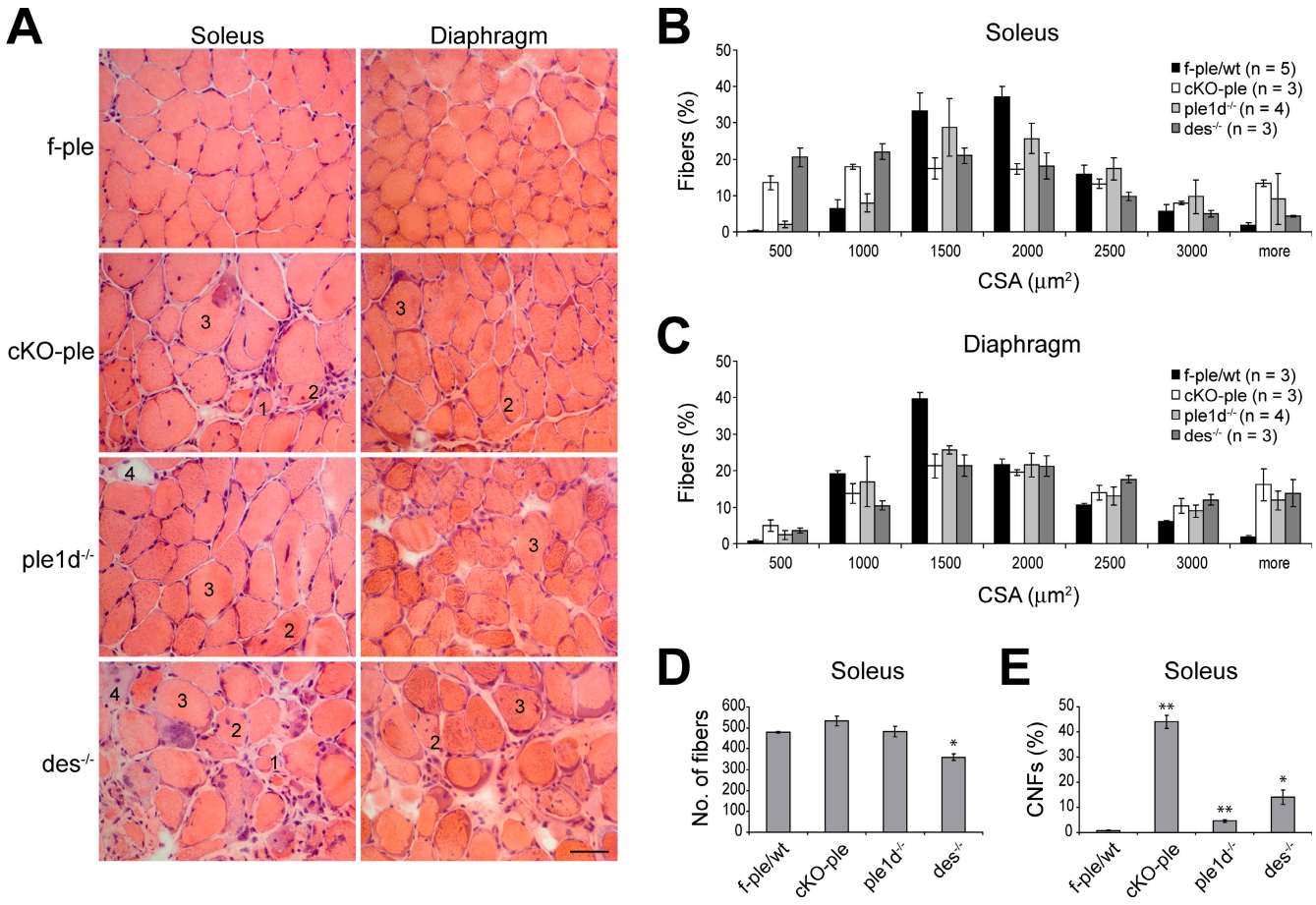

Figure 5. **Comparison of pathological alterations in 1-yr-old cKO-ple, ple1d$^{-/-}$, and des$^{-/-}$ mice.** (A) H & E analysis of soleus and diaphragm. Atrophic (1), centrally nucleated (2), hypertrophic (3), and necrotic fibers (4) are indicated. Bar, 50 µm. (B and C) Bar graphs showing CSAs of control and mutant fibers in soleus (B) and diaphragm (C). (D and E) Quantification of total numbers of fibers (D) and of CNFs (E) in soleus from at least three mice per genotype. Data represent means ± SEM. *, P < 0.05; **, P < 0.01.

and mitochondrial network organization. To study muscle-specific functions of these isoforms, we generated two independent plectin isoform knockout mouse lines: 1d-deficient (ple1d$^{-/-}$) and 1b-deficient (ple1b$^{-/-}$; Fig. S4, available at http://www.jcb.org/cgi/content/full/jcb.200711058/DC1; and unpublished data). Skeletal muscle samples from these mice were analyzed, along with similar specimens from des$^{-/-}$ and cKO-ple mice and a previously established plectin isoform 1 knockout (ple1$^{-/-}$) mouse model (Abrahamsberg et al., 2005).

As assessed by H & E staining, soleus specimens from 1-yr-old ple1$^{-/-}$ and ple1b$^{-/-}$ mice showed no obvious pathological alterations (Fig. S5, available at http://www.jcb.org/cgi/content/full/jcb.200711058/DC1), whereas in 1-yr-old ple1d$^{-/-}$ as well as in cKO-ple and des$^{-/-}$ muscles, necrotic, centrally nucleated, hypertrophic, and atrophic fibers were seen (Fig. 5 A and not depicted). Quantification of cross-sectional areas (CSAs) of fibers consistently revealed high fractions of hypertrophic and small-diameter fibers in soleus and diaphragm of mutant mice (Fig. 5, B and C, respectively). However, although the amount of small diameter fibers was particularly high in both cKO-ple and des$^{-/-}$ soleus (Fig. 5 B), the total number of fibers was markedly reduced in des$^{-/-}$ (~360) and slightly increased in cKO-ple (~530) soleus (Fig. 5 D). The corresponding numbers in control and ple1d$^{-/-}$ samples reached ~480 in both cases. Furthermore, the number of CNFs was exceptionally high (~44%) in cKO-ple soleus (vs. 0.8% in the control), whereas in des$^{-/-}$ and ple1d$^{-/-}$ mice, these numbers were markedly lower, reaching ~14 and ~5%, respectively (Fig. 5 E). Relatively low numbers of CNFs in ple1d$^{-/-}$ compared with cKO-ple soleus indicated that the remaining plectin isoforms were able to preserve ple1d$^{-/-}$ muscles from more extensive fiber death. Moreover, considering that plectin was present in regenerating fibers of cKO-ple mice (Fig. S1 C), the low number of CNFs and a decrease in total numbers of fibers in des$^{-/-}$ muscle pointed to inefficient fiber regeneration due to the loss of functional IF networks in satellite cells and/or myoblasts.

Desmin IFs are organized in a plectin isoform–dependent manner

Although in the cases of ple1$^{-/-}$, ple1b$^{-/-}$, and des$^{-/-}$ mice, on cryosections of soleus, antibodies reactive with all isoforms of plectin showed regular Z-disk arrays extending to the sarcolemma, in ple1d$^{-/-}$ muscles, they revealed only sarcolemmal staining (Fig. 6 A, arrow) and dotty remnants in the interior of fibers (Fig. 6 A, arrowheads). Plectin 1d deficiency consistently resulted in aggregation of desmin IFs (Fig. 6 C, a) as well as mitochondria

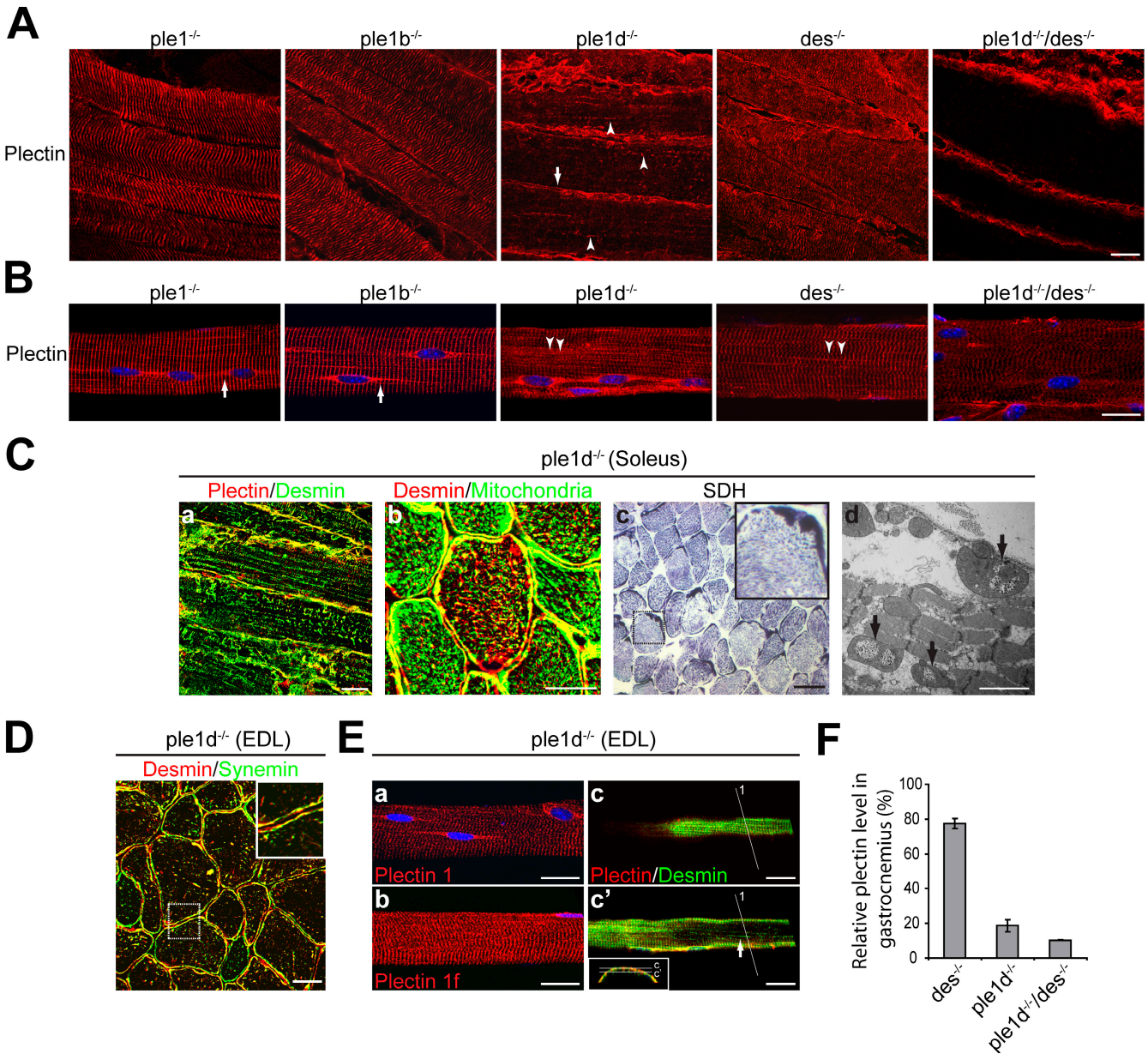

Figure 6. **Plectin isoform–dependent organization of desmin IFs.** (A) Longitudinal sections of soleus immunostained using antiserum 46 to plectin. Striated plectin patterns are observed in ple1$^{-/-}$, ple1b$^{-/-}$, and des$^{-/-}$samples; in ple1d$^{-/-}$ and ple1d$^{-/-}$/des$^{-/-}$ samples, such patterns are missing. The arrow and arrowheads in the ple1d$^{-/-}$ panel represent plectin-positive sarcolemmal and interior dotlike structures, respectively. Note that the interior of ple1d$^{-/-}$/des$^{-/-}$ fibers is completely devoid of plectin-positive signals. (B) Teased fibers of EDL were immunostained as in A. Note, the signal associated with longitudinal perinuclear structures was decreased in ple1$^{-/-}$ compared with ple1b$^{-/-}$ fibers (arrows). Also, costameres were focally disorganized in ple1d$^{-/-}$ and des$^{-/-}$ samples (arrowheads). (C) Ple1d$^{-/-}$ soleus sections double immunolabeled for plectin and desmin (a), desmin and mitochondria (b), or stained for SDH (c). Inset shows subsarcolemmal aggregation of mitochondria in a magnified view of the boxed area. The electron micrograph in panel d shows internal lysis of enlarged mitochondria in the subsarcolemmal region (arrows). (D) Ple1d$^{-/-}$ EDL cross section double immunolabeled for desmin and synemin revealing aggregates in the interior of fibers and largely unaffected sarcolemmal regions (see also inset, a magnified view of the boxed area). (E) Immunofluorescence microscopy of teased ple1d$^{-/-}$ fibers (EDL) using antibodies as indicated. In panels a and b, note the largely unaffected perinuclear and costameric patterns of plectin 1 and 1f, respectively. Panels c and c′ represent sequential confocal sections of one fiber. An optical cross section of this fiber (marked 1) is shown as an inset in panel c′, with horizontal lines indicating the positions of the planes shown in panels c and c′. Note the costameric patterns lacking aggregates in panel c and that desmin aggregates in the interior part of the fiber in panel c′ (arrow). Bars: (A; B; C, a and b; D; and E) 20 µm; (C, c) 50 µm; (C, d) 2 µm. (F) Quantitative immunoblotting of plectin in gastrocnemius lysates from different mouse mutants. Data, relative to WT samples (100%), represent the means ± SEM of three experiments.

(Fig. 6 C, b and c). Moreover, compromised respiratory activity (Table S1, available at http://www.jcb.org/cgi/content/full/jcb.200711058/DC1) and lysis of mitochondria (Fig. 6 C, d) were observed. The dotlike remnants of plectin-positive Z-disk structures observed in ple1d$^{-/-}$ mice (Fig. 6 A, arrowheads) were found associated with both desmin IF aggregates (Fig. 6 C, a) and mitochondrial accumulations (not depicted), and in contrast to cKO-ple fibers, both types of aggregates overlapped in most of the fibers (compare Fig. 6 C, b, with Fig. 4 B, c). Furthermore, desmin IFs and mitochondria usually formed much larger

aggregates in the cytoplasm of cKO-ple compared with ple1d$^{-/-}$ mice (compare Fig. 4 A, c, with Fig. 6 C, c; and Fig. 4 B, c, with Fig. 6 C, b).

In ple1d$^{-/-}$ muscles, desmin and synemin IFs coaggregated in the interior of fibers (Fig. 6 D). In contrast, the sarcolemmal localization seemed to be preserved (compare the inset in Fig. 6 D with the insets in Fig. 2 C, c and d). To further investigate the localization of plectin at the sarcolemma, ple1$^{-/-}$, ple1b$^{-/-}$, ple1d$^{-/-}$, and des$^{-/-}$ EDLs were teased into single fibers. As shown in Fig. 6 B, the sarcolemmal patterns were largely unaffected, except for a slightly decreased perinuclear plectin signal in the case of ple1$^{-/-}$ compared with ple1b$^{-/-}$ (arrows), and apparent misalignments of costameres in the case of ple1d$^{-/-}$ and des$^{-/-}$ mice (arrowheads). The preserved plectin signals at perinuclear regions and costameres of ple1d$^{-/-}$ teased fibers were largely caused by the presence of plectin isoforms 1 and 1f, respectively, as revealed by isoform-specific antibodies to plectin (Fig. 6 E, a and b). Furthermore, the remaining plectin 1f apparently was able to preserve the peripheral (costameric; Fig. 6 E, c) but not the interior Z-disk–associated (Fig. 6 E, c′) desmin structures, as demonstrated by sequential optical confocal sections of the same fiber. This revealed that plectin 1d was necessary for desmin localization at Z-disks, whereas it was dispensable for the organization of desmin IFs at costameres.

Immunoblotting of gastrocnemius extracts revealed decreased expression levels of plectin not only in ple1d$^{-/-}$ (~19%), but also in des$^{-/-}$ samples (~77%) when compared with control (f-ple) levels (100%; Figs. 6 F and 7 A). This was consistent with the overall decreased plectin signal observed in des$^{-/-}$ soleus and EDL (Fig. 6, A and B) and suggested that the lack of desmin leads to decreased expression of one or more plectin isoforms. To investigate this phenotype in more detail, we generated a plectin 1d/desmin double knockout (ple1d$^{-/-}$/des$^{-/-}$) mouse line. The expression level of plectin in gastrocnemius from such mice reached only ~10%, which was markedly below the ple1d$^{-/-}$ level (Fig. 6 F). Furthermore, although a plectin-positive signal was still present at the sarcolemma of ple1d$^{-/-}$/des$^{-/-}$ muscle fibers (Fig. 6, A and B), dotlike remnants of plectin-positive Z-disk structures in the fiber interior, most probably representing plectin 1b, were no longer detectable (Fig. 6 A). This indicated that the more severe phenotype of des$^{-/-}$ relative to ple1d$^{-/-}$ mice (Fig. 5) was caused by the absence of desmin combined with decreased expression of plectin, especially the mitochondria-associated plectin isoform 1b.

Immunoblotting of ple1d$^{-/-}$ gastrocnemius revealed a phenotype similar to the one observed in cKO-ple mice, with marked increases in the levels of caveolin 3 and vinculin and reduced levels of ATP synthase, desmin, and synemin (Fig. 7 A). This phenotype was largely recapitulated in des$^{-/-}$ and ple1d$^{-/-}$/des$^{-/-}$ muscles; however, in these cases, synemin was undetectable (Fig. 7 A), as confirmed by immunofluorescence microscopy (not depicted). Furthermore, the unaffected pattern of desmin IF networks underneath the sarcolemma as revealed in teased fibers from ple1d$^{-/-}$ EDL, was accompanied by unaffected costameric distribution of β-DG, caveolin 3, nNOS, and syntrophin (Fig. 7 B), which suggests that the presence of plectin 1f is crucial for maintaining the organization of costameres.

Plectin 1d anchors the contractile apparatus to the plectin 1f/desmin network–based costameric lattice

Our histological analysis revealed a significantly higher fraction of hypertrophic fibers in the soleus and diaphragm of cKO-ple, ple1d$^{-/-}$, and des$^{-/-}$ mice compared with control mice (Fig. 5, A–C). We hypothesized that hypertrophy could be caused by shattered myofibril cohesion and sarcolemmal anchorage due to the absence of functional plectin 1d and desmin IF arrays. In agreement with this notion, light microscopy of ple1d$^{-/-}$ soleus revealed frequent detachments of the sarcolemma from α-actinin–positive Z-disks (Fig. 7 C, arrows) and an accumulation of mitochondria underneath the sarcolemma (Fig. 7 C, arrows) and in between myofibrils (Fig. 7 C, arrowheads). Also, electron microscopy (Fig. 7 D, asterisk) and toluidine blue staining revealed detachments of the sarcolemma in ~45% of ple1d$^{-/-}$ soleus fibers versus ~5% in wild-type (WT) samples (Fig. 7 D). To confirm this on the biochemical level, we probed microsomes for α-actinin. As revealed in Fig. 7 E, we found the α-actinin level to be decreased in ple1d$^{-/-}$ microsomes to ~72% of WT values, contrary to caveolin 3. α-actinin levels were reduced to an even higher extent in a microsomal fraction from ple1d$^{-/-}$/des$^{-/-}$ mice (to ~27%; Fig. 7 E), which suggests that plectin 1f and desmin arrays are necessary for the proper anchorage of α-actinin–based cytoskeleton to the sarcolemma. Given these data, we reasoned that Z-disk–associated plectin 1d not only anchors desmin IFs linking Z-disks but also those connecting the contractile apparatus to the plectin 1f/desmin network–based costameric lattice (see Fig. 8).

Discussion

In the present study, we show that plectin deficiency in striated muscle leads to altered levels and localization of costameric and IF proteins, dysfunction and loss of mitochondria, and plectin isoform–dependent aggregation of desmin IFs at distinct locations. Our data demonstrate that plectin controls desmin IF and mitochondria network organization in muscle fibers with severe consequences for mitochondrial function and proper energy supply. Additionally, we show that plectin and desmin networks may play a profound role in fiber regeneration. Based on these results, we suggest that the progressive muscle wasting observed in EB-MD patients (Pfendner et al., 2005) is caused by fiber death combined with inefficient regeneration.

Different etiology of desmin aggregates in EB-MD and desmin-related myopathies (DRMs)

Disrupted desmin patterns have previously been described in patients with DRMs, which are mainly caused by mutations in desmin (Goldfarb et al., 1998; Munoz-Marmol et al., 1998) and αB-crystallin (Vicart et al., 1998) genes, and in a few cases of EB-MD (Gache et al., 1996; Schröder et al., 2002; McMillan et al., 2007). Our results strongly suggest that DRM and EB-MD have different etiology. DRM is caused by either aberrant filament assembly or a lack of the chaperon-like functions provided by αB-crystallin that normally prevent desmin aggregation under

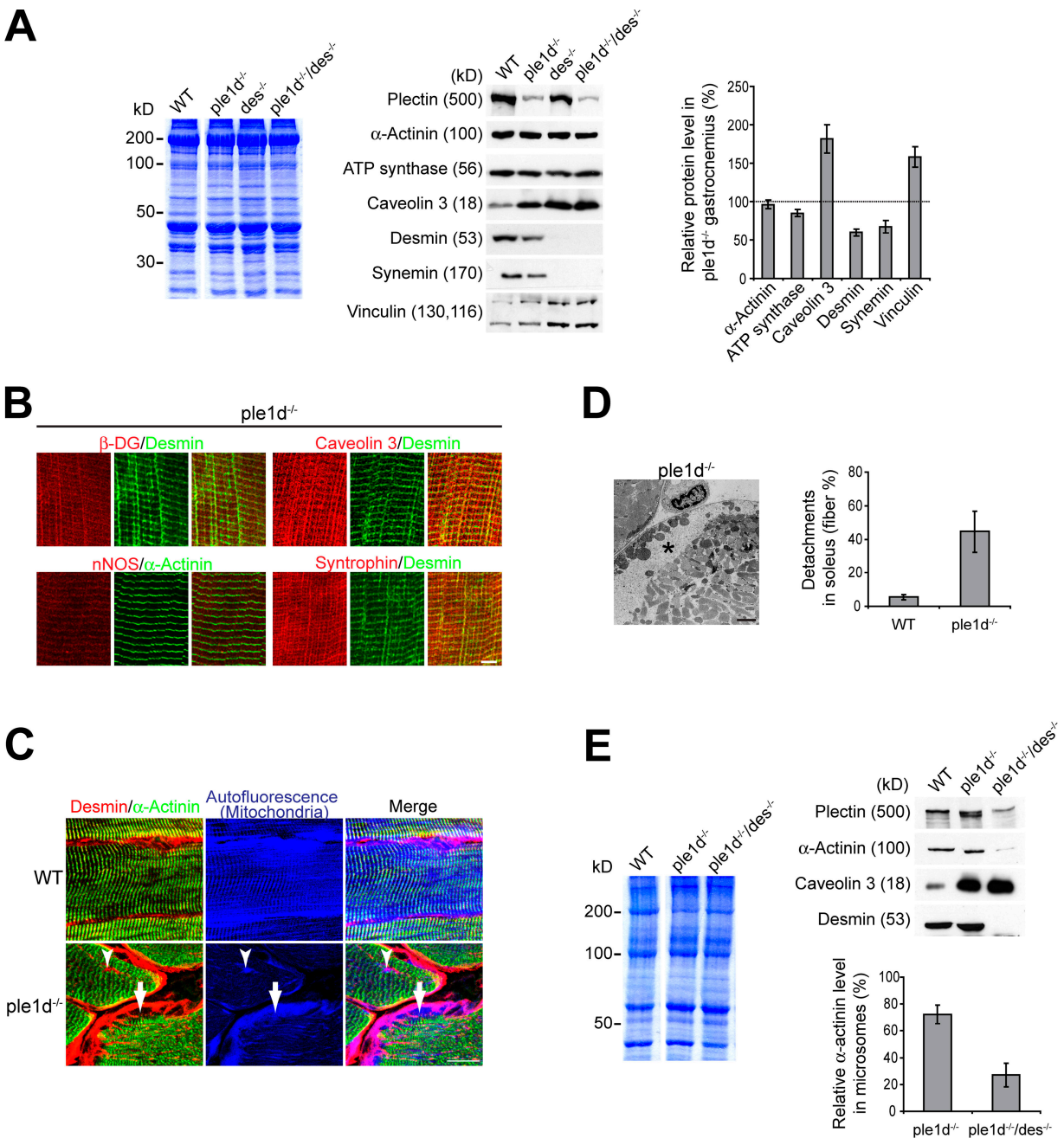

Figure 7. **Plectin 1d integrates the contractile apparatus, whereas plectin 1f anchors desmin IFs to the sarcolemma.** (A) Quantitative immunoblotting of gastrocnemius WT, ple1d$^{-/-}$, des$^{-/-}$, and ple1d$^{-/-}$/des$^{-/-}$ lysates using antibodies to the proteins indicated. Band intensities of ple1d$^{-/-}$ samples were evaluated densitometrically relative to WT signals from three mice per genotype. (B) Immunofluorescence microscopy of teased fibers (EDL) from a 4-mo-old ple1d$^{-/-}$ mouse revealing a largely unaffected costameric lattice. (C) Longitudinal sections of WT and ple1d$^{-/-}$ soleus double immunostained for desmin and α-actinin, and visualization of mitochondria by autofluorescence. Note: (1) the desmin-stained sarcolemma is detached from the sarcomeric α-actinin–positive cytoskeleton, (2) the space between the sarcolemma and the contractile apparatus is filled with autofluorescent green mitochondria (arrows), and (3) desmin IFs and mitochondria accumulate between α-actinin–stained myofibrils (arrowheads). (D) Electron micrograph of soleus showing detachment of the sarcolemma (asterisk) in a ple1d$^{-/-}$ fiber; the quantification of fibers showing detachments was performed as in Fig. 1 C. (E) Immunoblotting of microsomes from WT, ple1d$^{-/-}$, and ple1d$^{-/-}$/des$^{-/-}$ muscles and quantification of α-actinin in microsomes relative to WT signal (100%). Coomassie-stained gels in A and E were used as loading controls. Graphs represent mean values ± SEM. Bars: (B) 5 µm; (C) 20 µm; (D) 2 µm.

stress conditions (Goldfarb et al., 2004). In contrast, in the absence of plectin, desmin aggregation is apparently a consequence of missing connections between desmin IFs and other structures, loose (unanchored) filament ends, or both. Consistent with this notion, we observed that plectin was properly localized at Z-disks and costameres of des$^{-/-}$ mice. Importantly, because cKO-ple mice were used in our study, we could rule out the possibility that desmin coaggregated with self-aggregating plectin mutant forms, as it might be the case in EB-MD patients (Bauer et al., 2001). On this basis, our data suggest that plectin plays a dominant role in desmin IF network organization in muscle fibers.

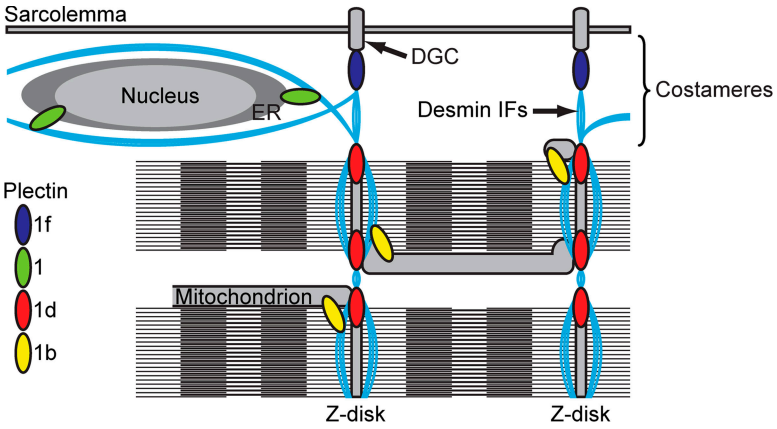

Figure 8. **Scheme depicting the different anchoring functions proposed for the four major plectin isoforms expressed in skeletal muscle.** Plectin 1d, 1f, 1b, and 1 link desmin IFs with Z-disks, costameres (DGC), mitochondria, and the outer nuclear/ER membrane system, respectively.

Do desmin aggregates poison muscle?

As we observed different patterns of aggregate formation in cKO-ple and ple1d$^{-/-}$ mice, differences in the progressivity of the observed phenotypes could be explained by the toxicity of IF aggregates. The involvement of IF aggregates in cell death was implicated not only in DRM and Alexander's disease but also in neurodegenerative diseases such as amyotrophic lateral sclerosis and Charcot-Marie-Tooth diseases. Moreover, in Alzheimer's and Parkinson's diseases, IFs were found to be a component of the inclusions (Cairns et al., 2004). Although the toxicity of aggregates remains elusive, it could be that abnormal proteins interact and recruit other cellular components and thus affect homeostasis. Another possibility is that aggregates cause aberrant protein turnover by inhibiting the proteasome or altering autophagy (Rubinsztein, 2006). The cumulative processes of either of these events could account for the observed differences in phenotypes of cKO-ple and ple1d$^{-/-}$ mice.

Plectin 1d integrates the contractile apparatus, whereas plectin 1f organizes the costameric lattice

Our studies on plectin isoform–specific knockout mice revealed that plectin 1d maintains the integrity of muscle fibers at the level of Z-disks by anchoring desmin IFs to adjacent myofibrils and connecting the contractile apparatus as a whole to costamere-associated desmin IFs (Fig. 8). This model is supported by our previous study showing that GFP–plectin 1d fusion proteins expressed in myotubes were exclusively localized at Z-disks (Rezniczek et al., 2007). Moreover, in ple1d$^{-/-}$ samples, the localization of costameric marker proteins appeared unaffected, and desmin aggregates were observed only in the fiber interior, whereas changes in the organization of the costameric lattice were observed in cKO-ple mice and also in des$^{-/-}$ mice (O'Neill et al., 2002). This suggests that in the absence of plectin 1d, the remaining unaffected costameric isoform 1f was able to anchor desmin IFs to the DGC (Fig. 8) and thus provided a scaffold for other costameric proteins. The observed hypertrophy in cKO-ple, ple1d$^{-/-}$, and des$^{-/-}$ muscles presumably was a consequence of reduced compactness of the fiber interior due to the absence of integrating plectin and desmin IF arrays. However, it cannot be excluded that this phenotype was caused by the activation of NFAT or MEF2 family members, which are known to cause muscle hypertrophy in response to mechanical stress (Olson and Williams, 2000).

Measurements of creatine kinase activity in serum of either sedentary or exercised mice revealed no significant differences between f-ple and cKO-ple mice. Similarly, no apparent accumulation of EBD in the fiber interior of cKO-ple fibers was detected. These results correspond with a previous study (Haubold et al., 2003) showing no increase in creatine kinase serum activity in des$^{-/-}$ mice. Based on our immunoblotting data in gastrocnemius lysates and microsomes showing increased amounts of costameric marker proteins, we hypothesize that the apparently unaffected integrity of the sarcolemma in both cKO-ple and des$^{-/-}$ mice is caused by the increased recruitment of DGC and integrin complex constituents. This interpretation is consistent with the observation that increased sarcolemmal permeability in mdx muscles (Straub et al., 1997) is accompanied by a reduction of DGC components (Ohlendieck and Campbell, 1991).

Evidence for plectin 1b linking mitochondria with desmin IFs

In ple1d$^{-/-}$ mice, we found residual plectin associated with mitochondria and colocalization of aggregated desmin and mitochondrial aggregates in-between myofibrils. Such colocalization was rarely observed in the case of cKO-ple fibers. This difference could be explained if one assumes that the localization of plectin 1b in ple1d$^{-/-}$ mice was unaffected and that the protein was still bound to mitochondria (Fig. 8). This would be in agreement with a previous study that revealed the association of plectin with two different populations of IFs in the interior of muscle fibers (Reipert et al., 1999), namely the prominent IF belt structure along Z-disks and IFs spanning from myofibrils to adjacent mitochondria. Moreover, forced expression of plectin 1b in cultured cells showed colocalization of this isoform with mitochondria (Rezniczek et al., 2003, 2007), and an abnormal morphology of mitochondria was observed in plectin 1b–deficient fibroblasts (unpublished data).

Mitochondrial aggregates have previously been revealed in des$^{-/-}$ mice (Milner et al., 2000) and in one case of EB-MD (Schröder et al., 2002). However, the involvement of plectin and desmin in mitochondrial network organization is still controversial, as other EB-MD patients revealed no or only marginal disruption of mitochondria distribution (McMillan et al., 2007).

The present study showed a severe disorganization of mitochondrial networks in muscles from plectin-deficient mice. Furthermore, markedly reduced mitochondria levels, a decrease in mitochondrial complex I activity, and a loss of creatine kinase coupling with adenine nucleotide translocator (Table S1) were observed. Because our data indicate that mitochondria are anchored into desmin network arrays via plectin, it is possible that the absence of either plectin or desmin results in insufficient spatial separation of mitochondria leading to their aggregation. Alternatively, plectin isoform 1b may interact directly or indirectly with mitochondrial effectors and thereby regulate their functions.

In conclusion, our studies uncovered a crucial role of plectin in preserving the functional integrity of the skeletal muscle fiber. The results indicate that plectin deficiency causes dysfunction and loss of mitochondria leading to energy deprivation and fiber death. Using a conditional knockout mouse model in combination with isoform-specific knockouts, we demonstrated that the integrity of the desmin IF network depends on plectin isoform–mediated specific targeting of filaments to distinct docking sites. These multiple new knockout mouse models may also be useful for developing therapies for plectin- and desmin-related myopathies.

Materials and methods

Mice

All experiments involving animals were performed in agreement with Austrian Federal Government laws and regulations. cKO-ple mice ($ple^{\Delta/-}$, $ple^{\Delta/\Delta}$) were obtained through multiple crossing steps. A mouse line hemizygous for the MCK-Cre transgene (provided by C.R. Kahn, Joslin Diabetes Center and Harvard Medical School, Boston, MA; Bruning et al., 1998) was first bred to heterozygous plectin-null mice ($ple^{+/-}$; Andrä et al., 1997). Heterozygous mice positive for the Cre transgene were then crossed with mice homozygous for the floxed allele ($ple^{f/f}$; Ackerl et al., 2007). $Ple^{\Delta/-}$, $ple^{f/-}$, and $ple^{f/+}$ mice obtained were used for primary analyses. Subsequently, $ple^{\Delta/-}$ mice were bred to $ple^{f/-}$ mice, and $ple^{\Delta/\Delta}$, $ple^{\Delta/-}$, $ple^{f/f}$, and $ple^{f/-}$ mice generated were used for further analyses. No differences between $ple^{\Delta/\Delta}$ and $ple^{\Delta/-}$ or among f-ple ($ple^{f/f}$, $ple^{f/+}$, and $ple^{f/-}$) were observed. f-ple mice were used as control animals in all experiments involving cKO-ple mice.

For generating plectin isoform 1d–deficient mice, a targeting construct was prepared that enabled elimination of the DNA region harboring the first coding exon 1d. This region was replaced by a neomycin resistance cassette (neo) flanked by two loxP sites. The targeting vector was constructed by joining a 5.2-kb fragment (flanked by BamHI and SpeI sites and located upstream of exon 1d) and a 4.5-kb fragment (flanked by an introduced EcoRI and XmaI site and located downstream of exon 1d) to a thymidine kinase promoter-driven neo cassette (provided by M. Kraus, Institute for Genetics, University of Cologne, Cologne, Germany). The linearized targeting vector was electroporated into embryonic stem cells (line E14.1; Andrä et al., 1997; Abrahamsberg et al., 2005). G418-resistant colonies of cells heterozygous for the correctly targeted allele were isolated and identified by Southern blot analysis. Germ line chimeras obtained were bred to C57BL/6 females to obtain F1 mice heterozygous for the plectin 1d deletion. Genotyping of offspring was performed by Southern blot analysis of tail DNA by digestion with EcoRI and hybridization to α-^{32}P–labeled probe located outside of the homology arm. $Ple1d^{-/-}/des^{-/-}$ mice were generated by breeding $ple1d^{-/-}$ mice to $des^{-/-}$ mice (Li et al., 1996). $Ple1b^{-/-}$ mice were generated and phenotypically analyzed similar to plectin $1^{-/-}$ mice (Abrahamsberg et al., 2005).

RNase protection assays

RNase protection assays were performed as described previously (Elliott et al., 1997). cDNA sequences used as probes were PCR subcloned into pSP64 (Promega) using primers flanked with suitable restriction sites. Probes specific for ribosomal protein S16 and for plectin exons 1d and 32 have been described previously (Fuchs et al., 1999).

Voluntary wheel-running and serum creatine kinase measurements

Mice were placed into cages (140 × 207 × 367 mm) that were equipped with a metal hamster wheel (145 mm in diameter; PetSmart) attached to a bicycle computer. In the course of the experiments, distance and running time were recorded daily. Mean speed was obtained from the distance and time values. Serum creatine kinase was determined spectrophotometrically using creatine kinase reagent (Procedure No. 47-UV; Sigma-Aldrich).

Antibodies

The following primary antibodies were used for immunofluorescence microscopy (IF) and immunoblotting (IB): mouse mAb EA-53 to α-actinin (IF and IB; Sigma-Aldrich); mouse mAb 7H10 to ATP synthase (IB; Invitrogen); rat mAb MB1.2 to integrin β1 (IB; Millipore); mouse mAb 43DAG1/8D5 (IB; Novocastra) and rabbit antiserum (AS) 1710 (IF; provided by S.J. Winder, University of Sheffield, Sheffield, UK; Ilsley et al., 2001) to β-DG; mouse mAb (clone 26) to caveolin-3 (IF and IB; BD Biosciences); mouse mAb 7H8.2C12 to cytochrome *c* (IB; BD Biosciences); guinea pig AS to mouse liver cytokeratin 8 (Denk et al., 1982); mouse mAbs DE-R-11 (IF and IB) and D33 (IF; Dako) and rabbit AS V2022 (IF and IB; Biomeda) to desmin; mouse mAbs DP-2.15, DP-2.17, and DP-2.20 to desmoplakin (IF; Progen Pharmaceuticals Limited); mouse mAb DY4/6D3 to dystrophin (IB; Novocastra); rabbit AS R-20 to NOS1 (IF and IB; Santa Cruz Biotechnology, Inc.); mouse mAb 1D6 to OxPhos Complex IV subunit I (IF; Invitrogen); rabbit AS 9 (IB) and rabbit AS 46 (IF; Andrä et al., 2003) to plectin; rabbit AS to plectin isoform 1 (IF; Abrahamsberg et al., 2005); rabbit AS to plectin isoform 1f (IF; Rezniczek et al., 2007); mouse mAb 20B12 to porin (IB; Invitrogen); rabbit AS SYNC-FP to syncoilin (IF; provided by K.E. Davies, University of Oxford, Oxford, UK; Newey et al., 2001); rabbit AS syn3 to synemin (IF and IB; Titeux et al., 2001); mouse mAb 1351 to syntrophin (IF and IB; Affinity BioReagents); mouse mAb D8B7 to α-II spectrin (IB; Covance); mouse mAb 8D4 to talin (IB; Sigma-Aldrich); rabbit AS RAB5 to utrophin (IB; provided by S.J. Winder; James et al., 2000); and mouse mAb VIN-11-5 to vinculin (IB; Sigma-Aldrich). Secondary antibodies used were: goat Cy3 anti–mouse, goat Rhodamine red anti–rabbit, goat Cy5 anti–rabbit, donkey Cy5 anti–mouse, donkey Cy3 anti–guinea pig (Jackson ImmunoResearch Laboratories), and streptavidin Alexa 633 (Invitrogen) for IF; and goat anti–rabbit and anti–mouse HRP-conjugated IgGs (Jackson ImmunoResearch Laboratories) for IB.

Immunofluorescence microscopy

Teased fibers were prepared and processed as described previously (Rezniczek et al., 2007). Thin sections (5 µm) were obtained from tissues that were snap frozen in liquid nitrogen–cooled isopentane. The staining procedure was performed with the MOM Basic kit (Vector Laboratories). After incubation with secondary antibodies, samples were mounted in Mowiol and viewed in a fluorescence microscope (Axiovert 100M; Carl Zeiss, Inc.) using either a Plan-Apochromat 63× 1.4 NA or Plan-Apochromat 100× 1.4 NA objectives (Carl Zeiss, Inc.). Images were recorded using the LSM510 module (Carl Zeiss, Inc.) and the LSM510 software package (version 3.2 SP2; Carl Zeiss, Inc.) and processed using the LSM Image Browser (generation of projections of confocal stacks, brightness and contrast adjustments; version 3.2; Carl Zeiss, Inc.) and Photoshop CS2 (brightness and contrast adjustments, cropping, and splitting of color channels; Adobe).

Histology

H & E, Sirius red, and toluidine blue stainings were performed using standard procedures. Fiber type was determined by myosin ATPase staining (pH 4.54). CSAs of fibers were measured using ImageJ software. To obtain SDH stainings, frozen sections (5 µm) were incubated in 50 mM Tris/HCl, pH 7.4, 0.2 M sodium-succinate, 50 mM $MgCl_2$, and 2 mg/ml Nitroblue tetrazolium (NBT) for 1 h at 37°C. Unbound NBT was removed by washing the samples in increasing (30, 60, and 90%) and then decreasing (90, 60, and 30%), acetone concentrations. Slides were rinsed with ddH_2O and mounted in Mowiol. COX staining was performed by incubating samples in 0.05% 3,3′-diaminobenzidine tetrahydrochloride, 0.1% cytochrome *c*, 0.02% catalase, 7.5% sucrose, and 80 mM phosphate buffer, pH 7.4, for 1 h at 37°C. The slides were then dehydrated, cleared with xylene, and mounted in Histofluid (Marienfeld). Samples were viewed in an Axiophot microscope (Carl Zeiss, Inc.) using either Plan-Neofluar 10× 0.3 NA or Plan-Neofluar 20× 0.5 NA objectives (Carl Zeiss, Inc.). Images were recorded using AxioVision 4.4 software (Carl Zeiss, Inc.) and processed using Photoshop CS2 (brightness and contrast adjustments).

Immunoblotting

Dissected muscles were homogenized and the amount of total protein was determined as described previously (Chopard et al., 2000). Microsomal

fractions were prepared from pooled hind-leg muscles from at least three mice per genotype as described previously (Rezniczek et al., 2007). Densitometrical analysis was performed with QuantiScan 1.5 (Biosoft).

Electron microscopy

Adult mice were fixed in situ by perfusion with 2.5% paraformaldehyde, 0.5% glutaraldehyde, or 4% pararaformaldehyde in PBS, pH 7.5, at 37°C via intercardiac puncture. Muscle tissues were dissected and immersion-fixed with 3% glutaraldehyde in Sorensen's buffer at 4°C overnight. Post-fixation was performed in 1.5% OsO_4 for 90 min followed by dehydration in ethanol and embedding in epoxy resin (Agar 100). Thin sections for ultrastructural assessment were cut with an ultramicrotome (Ultracut S; Leica). Sections were mounted on copper grids, counterstained with uranyl acetate and lead citrate, and examined at either 60 or 80 kV in an electron microscope (JEM-1210; JEOL, Ltd.). Images of ple1d$^{-/-}$ tissues were photographically recorded on negatives, whereas images of the cKO-ple tissues were acquired by using a digital camera (MegaView III) for the wide-angle port of the transmission electron microscopy and analySIS FIVE software (Soft Imaging System, GmbH).

Measurements of mitochondrial complex activities

Measurements of mitochondrial complex activities were performed on isolated mitochondria (ple1d$^{-/-}$) or muscles (cKO-ple). Soleus muscle samples were incubated for 30 min in ice-cold 180 mM KCl, 10 mM EDTA, pH 7.4, and 0.1% trypsin. Homogenization was then performed in the same solution without trypsin. The filtered supernatant was centrifuged and the pellet was resuspended in 180 mM KC1, pH 7.4, and homogenized again, and the final mitochondrial pellet was resuspended in the same buffer.

The specific activity of complex I (NADH–Q1) was measured by following the oxidation of NADH in the presence of CoQ1, and complex IV (COX) activities were monitored by measuring oxidation of ferrocytochrome *c* (Kuznetsov et al., 1998). Citrate synthase activities were measured by following the reduction of 5,5′dithiobis (2-nitrobenzoic acid; DTNB) by CoASH, liberated by the citrate synthase reaction in the presence of oxaloacetate and acetyl-CoA.

In situ respiratory measurements of mitochondria

Soleus muscle fibers were teased in 50 mM MES, pH 7.1, 3 mM KH_2PO_4, 20 mM taurin, 0.5 mM DTT, 20 mM imidazole, 9.5 mM $MgCl_2 \times 6\ H_20$, 5.26 mM ATP, 15 mM creatine phosphate, 0.1 M K_2Ca-EGTA, 0.1 M K_2EGTA, and 5.6 mM ATP-Mg, and subsequently incubated in 0.5% saponin for 30 min at 4°C. Samples were then washed three times in 60 mM Tris, pH 7.4, 10 mM KH_2PO_4, 60 mM KCl, 110 mM mannitol, 0.5 mM Na-EDTA, and 0.022% BSA (respiration buffer) for 10 min at 4°C and then transferred to fresh respiration buffer without BSA. Subsequently, saponin-skinned fibers were transferred to respiration buffer (supplemented with 0.5 mM DTT, 3.3 mM $MgCl_2$, 5 mM malate, and 10 mM glutamate) equilibrated with air (25°C). The rate of oxygen consumption was measured using a high-resolution oxygraph (Oroboros). The determination of the apparent K_M values for ADP in skinned fibers was performed by adding increasing concentrations of ADP. Creatine kinase and adenine nucleotide translocator coupling was determined by adding solid creatine to a final concentration of 50 mM into the reaction mixture before the first ADP addition. The respiration rates were plotted as a function of ADP concentration and the K_M and maximal rate of oxygen consumption (v_{max}) values were calculated using the ENZFIT program (Elsevier-Biosoft).

Online supplemental material

Fig. S1 shows abolished plectin expression in mature striated muscle cells of cKO-ple mice. Fig. S2 shows survival curves, x-ray images, and voluntary wheel-running analysis of f-ple and cKO-ple mice. Fig. S3 shows representative serial sections from f-ple and cKO-ple mice stained for SDH, COX, H & E, and myosin ATPase. Fig. S4 describes generation and characterization of plectin 1d–deficient mice. Fig. S5 shows the unaffected morphological appearance of ple1$^{-/-}$ and ple1b$^{-/-}$ soleus fibers. Table S1 (top) describes respiratory parameters (decreased K_M value for ADP) of saponin-permeabilized soleus fibers of ple1d$^{-/-}$ mice indicating altered creatine kinase coupling. Table S1 (bottom) shows compromised NADH–Q1 reductase activity in isolated ple1d$^{-/-}$ mitochondria. Online supplemental material is available at http://www.jcb.org/cgi/content/full/jcb.200711058/DC1.

We thank C.R. Kahn for generously providing us with MCK-Cre mice, K.E. Davies, and S.J. Winder for donating antibodies, and C. Abrahamsberg for providing the ple1b$^{-/-}$ mouse line and for critical comments during the preparation of this manuscript.

This work was supported by grants F006-11 and P17862-B09 from the Austrian Science Research Fund.

Submitted: 12 November 2007
Accepted: 18 April 2008

References

Abrahamsberg, C., P. Fuchs, S. Osmanagic-Myers, I. Fischer, F. Propst, A. Elbe-Bürger, and G. Wiche. 2005. Targeted ablation of plectin isoform 1 uncovers role of cytolinker proteins in leukocyte recruitment. *Proc. Natl. Acad. Sci. USA.* 102:18449–18454.

Ackerl, R., G. Walko, P. Fuchs, I. Fischer, M. Schmuth, and G. Wiche. 2007. Conditional targeting of plectin in prenatal and adult mouse stratified epithelia causes keratinocyte fragility and lesional epidermal barrier defects. *J. Cell Sci.* 120:2435–2443.

Andrä, K., H. Lassmann, R. Bittner, S. Shorny, R. Fässler, F. Propst, and G. Wiche. 1997. Targeted inactivation of plectin reveals essential function in maintaining the integrity of skin, muscle, and heart cytoarchitecture. *Genes Dev.* 11:3143–3156.

Andrä, K., I. Kornacker, A. Jörgl, M. Zörer, D. Spazierer, P. Fuchs, I. Fischer, and G. Wiche. 2003. Plectin-isoform-specific rescue of hemidesmosomal defects in plectin (−/−) keratinocytes. *J. Invest. Dermatol.* 120:189–197.

Bauer, J.W., F. Rouan, B. Kofler, G.A. Rezniczek, I. Kornacker, W. Muss, R. Hametner, A. Klausegger, A. Huber, G. Pohla-Gubo, et al. 2001. A compound heterozygous one amino-acid insertion/nonsense mutation in the plectin gene causes epidermolysis bullosa simplex with plectin deficiency. *Am. J. Pathol.* 158:617–625.

Bellin, R.M., T.W. Huiatt, D.R. Critchley, and R.M. Robson. 2001. Synemin may function to directly link muscle cell intermediate filaments to both myofibrillar Z-lines and costameres. *J. Biol. Chem.* 276:32330–32337.

Bloch, R.J., Y. Capetanaki, A. O'Neill, P. Reed, M.W. Williams, W.G. Resneck, N.C. Porter, and J.A. Ursitti. 2002. Costameres: repeating structures at the sarcolemma of skeletal muscle. *Clin. Orthop. Relat. Res.*:S203–S210.

Bruning, J.C., M.D. Michael, J.N. Winnay, T. Hayashi, D. Horsch, D. Accili, L.J. Goodyear, and C.R. Kahn. 1998. A muscle-specific insulin receptor knockout exhibits features of the metabolic syndrome of NIDDM without altering glucose tolerance. *Mol. Cell.* 2:559–569.

Cairns, N.J., V.M. Lee, and J.Q. Trojanowski. 2004. The cytoskeleton in neurodegenerative diseases. *J. Pathol.* 204:438–449.

Capetanaki, Y., R.J. Bloch, A. Kouloumenta, M. Mavroidis, and S. Psarras. 2007. Muscle intermediate filaments and their links to membranes and membranous organelles. *Exp. Cell Res.* 313:2063–2076.

Chopard, A., F. Pons, P. Charpiot, and J.F. Marini. 2000. Quantitative analysis of relative protein contents by Western blotting: comparison of three members of the dystrophin-glycoprotein complex in slow and fast rat skeletal muscle. *Electrophoresis.* 21:517–522.

Denk, H., R. Krepler, E. Lackinger, U. Artlieb, and W.W. Franke. 1982. Biochemical and immunocytochemical analysis of the intermediate filament cytoskeleton in human hepatocellular carcinomas and in hepatic neoplastic nodules of mice. *Lab. Invest.* 46:584–596.

Elliott, C.E., B. Becker, S. Oehler, M.J. Castañón, R. Hauptmann, and G. Wiche. 1997. Plectin transcript diversity: identification and tissue distribution of variants with distinct first coding exons and rodless isoforms. *Genomics.* 42:115–125.

Ervasti, J.M. 2003. Costameres: the Achilles' heel of Herculean muscle. *J. Biol. Chem.* 278:13591–13594.

Fuchs, P., M. Zörer, G.A. Rezniczek, D. Spazierer, S. Oehler, M.J. Castañón, R. Hauptmann, and G. Wiche. 1999. Unusual 5′ transcript complexity of plectin isoforms: novel tissue-specific exons modulate actin binding activity. *Hum. Mol. Genet.* 8:2461–2472.

Gache, Y., S. Chavanas, J.P. Lacour, G. Wiche, K. Owaribe, G. Meneguzzi, and J.P. Ortonne. 1996. Defective expression of plectin/HD1 in epidermolysis bullosa simplex with muscular dystrophy. *J. Clin. Invest.* 97:2289–2298.

Goldfarb, L.G., K.Y. Park, L. Cervenakova, S. Gorokhova, H.S. Lee, O. Vasconcelos, J.W. Nagle, C. Semino-Mora, K. Sivakumar, and M.C. Dalakas. 1998. Missense mutations in desmin associated with familial cardiac and skeletal myopathy. *Nat. Genet.* 19:402–403.

Goldfarb, L.G., P. Vicart, H.H. Goebel, and M.C. Dalakas. 2004. Desmin myopathy. *Brain.* 127:723–734.

Haubold, K.W., D.L. Allen, Y. Capetanaki, and L.A. Leinwand. 2003. Loss of desmin leads to impaired voluntary wheel running and treadmill exercise performance. *J. Appl. Physiol.* 95:1617–1622.

Hijikata, T., T. Murakami, M. Imamura, N. Fujimaki, and H. Ishikawa. 1999. Plectin is a linker of intermediate filaments to Z-discs in skeletal muscle fibers. *J. Cell Sci.* 112:867–876.

Ilsley, J.L., M. Sudol, and S.J. Winder. 2001. The interaction of dystrophin with beta-dystroglycan is regulated by tyrosine phosphorylation. *Cell. Signal.* 13:625–632.

James, M., A. Nuttall, J.L. Ilsley, K. Ottersbach, J.M. Tinsley, M. Sudol, and S.J. Winder. 2000. Adhesion-dependent tyrosine phosphorylation of (beta)-dystroglycan regulates its interaction with utrophin. *J. Cell Sci.* 113:1717–1726.

Kuznetsov, A.V., K. Winkler, F.R. Wiedemann, P. von Bossanyi, K. Dietzmann, and W.S. Kunz. 1998. Impaired mitochondrial oxidative phosphorylation in skeletal muscle of the dystrophin-deficient mdx mouse. *Mol. Cell. Biochem.* 183:87–96.

Li, Z., E. Colucci-Guyon, M. Pincon-Raymond, M. Mericskay, S. Pournin, D. Paulin, and C. Babinet. 1996. Cardiovascular lesions and skeletal myopathy in mice lacking desmin. *Dev. Biol.* 175:362–366.

McMillan, J.R., M. Akiyama, F. Rouan, J.E. Mellerio, E.B. Lane, I.M. Leigh, K. Owaribe, G. Wiche, N. Fujii, J. Uitto, et al. 2007. Plectin defects in epidermolysis bullosa simplex with muscular dystrophy. *Muscle Nerve.* 35:24–35.

Milner, D.J., G. Weitzer, D. Tran, A. Bradley, and Y. Capetanaki. 1996. Disruption of muscle architecture and myocardial degeneration in mice lacking desmin. *J. Cell Biol.* 134:1255–1270.

Milner, D.J., M. Mavroidis, N. Weisleder, and Y. Capetanaki. 2000. Desmin cytoskeleton linked to muscle mitochondrial distribution and respiratory function. *J. Cell Biol.* 150:1283–1298.

Munoz-Marmol, A.M., G. Strasser, M. Isamat, P.A. Coulombe, Y. Yang, X. Roca, E. Vela, J.L. Mate, J. Coll, M.T. Fernandez-Figueras, et al. 1998. A dysfunctional desmin mutation in a patient with severe generalized myopathy. *Proc. Natl. Acad. Sci. USA.* 95:11312–11317.

Newey, S.E., E.V. Howman, C.P. Ponting, M.A. Benson, R. Nawrotzki, N.Y. Loh, K.E. Davies, and D.J. Blake. 2001. Syncoilin, a novel member of the intermediate filament superfamily that interacts with alpha-dystrobrevin in skeletal muscle. *J. Biol. Chem.* 276:6645–6655.

Ohlendieck, K., and K.P. Campbell. 1991. Dystrophin-associated proteins are greatly reduced in skeletal muscle from mdx mice. *J. Cell Biol.* 115:1685–1694.

Olson, E.N., and R.S. Williams. 2000. Remodeling muscles with calcineurin. *Bioessays.* 22:510–519.

O'Neill, A., M.W. Williams, W.G. Resneck, D.J. Milner, Y. Capetanaki, and R.J. Bloch. 2002. Sarcolemmal organization in skeletal muscle lacking desmin: evidence for cytokeratins associated with the membrane skeleton at costameres. *Mol. Biol. Cell.* 13:2347–2359.

Osmanagic-Myers, S., M. Gregor, G. Walko, G. Burgstaller, S. Reipert, and G. Wiche. 2006. Plectin-controlled keratin cytoarchitecture affects MAP kinases involved in cellular stress response and migration. *J. Cell Biol.* 174:557–568.

Pfendner, E., F. Rouan, and J. Uitto. 2005. Progress in epidermolysis bullosa: the phenotypic spectrum of plectin mutations. *Exp. Dermatol.* 14:241–249.

Reipert, S., F. Steinböck, I. Fischer, R.E. Bittner, A. Zeöld, and G. Wiche. 1999. Association of mitochondria with plectin and desmin intermediate filaments in striated muscle. *Exp. Cell Res.* 252:479–491.

Rezniczek, G.A., C. Abrahamsberg, P. Fuchs, D. Spazierer, and G. Wiche. 2003. Plectin 5′-transcript diversity: short alternative sequences determine stability of gene products, initiation of translation and subcellular localization of isoforms. *Hum. Mol. Genet.* 12:3181–3194.

Rezniczek, G.A., P. Konieczny, B. Nikolic, S. Reipert, D. Schneller, C. Abrahamsberg, K.E. Davies, S.J. Winder, and G. Wiche. 2007. Plectin 1f scaffolding at the sarcolemma of dystrophic (mdx) muscle fibers through multiple interactions with β-dystroglycan. *J. Cell Biol.* 176:965–977.

Rubinsztein, D.C. 2006. The roles of intracellular protein-degradation pathways in neurodegeneration. *Nature.* 443:780–786.

Schröder, R., W.S. Kunz, F. Rouan, E. Pfendner, K. Tolksdorf, K. Kappes-Horn, M. Altenschmidt-Mehring, R. Knoblich, P.F. van der Ven, J. Reimann, et al. 2002. Disorganization of the desmin cytoskeleton and mitochondrial dysfunction in plectin-related epidermolysis bullosa simplex with muscular dystrophy. *J. Neuropathol. Exp. Neurol.* 61:520–530.

Straub, V., J.A. Rafael, J.S. Chamberlain, and K.P. Campbell. 1997. Animal models for muscular dystrophy show different patterns of sarcolemmal disruption. *J. Cell Biol.* 139:375–385.

Thornell, L., L. Carlsson, Z. Li, M. Mericskay, and D. Paulin. 1997. Null mutation in the desmin gene gives rise to a cardiomyopathy. *J. Mol. Cell. Cardiol.* 29:2107–2124.

Titeux, M., V. Brocheriou, Z. Xue, J. Gao, J.F. Pellissier, P. Guicheney, D. Paulin, and Z. Li. 2001. Human synemin gene generates splice variants encoding two distinct intermediate filament proteins. *Eur. J. Biochem.* 268:6435–6449.

Ursitti, J.A., P.C. Lee, W.G. Resneck, M.M. McNally, A.L. Bowman, A. O'Neill, M.R. Stone, and R.J. Bloch. 2004. Cloning and characterization of cytokeratins 8 and 19 in adult rat striated muscle. Interaction with the dystrophin glycoprotein complex. *J. Biol. Chem.* 279:41830–41838.

Vicart, P., A. Caron, P. Guicheney, Z. Li, M.C. Prevost, A. Faure, D. Chateau, F. Chapon, F. Tome, J.M. Dupret, et al. 1998. A missense mutation in the alphaB-crystallin chaperone gene causes a desmin-related myopathy. *Nat. Genet.* 20:92–95.

Washabaugh, C.H., M.P. Ontell, J.A. Kant, and M. Ontell. 1999. Creatine kinase transcript accumulation: effect of nerve during muscle development. *Dev. Dyn.* 215:285–296.

Wiche, G. 1998. Role of plectin in cytoskeleton organization and dynamics. *J. Cell Sci.* 111:2477–2486.

Yang, Z., N.E. Bowles, S.E. Scherer, M.D. Taylor, D.L. Kearney, S. Ge, V.V. Nadvoretskiy, G. DeFreitas, B. Carabello, L.I. Brandon, et al. 2006. Desmosomal dysfunction due to mutations in desmoplakin causes arrhythmogenic right ventricular dysplasia/cardiomyopathy. *Circ. Res.* 99:646–655.